PCCP

View Online
Dynamic Article Links

Cite this: *Phys. Chem. Chem. Phys.*, 2011, **13**, 7024–7036

www.rsc.org/pccp

PAPER

VUV state-selected photoionization of thermally-desorbed biomolecules by coupling an aerosol source to an imaging photoelectron/photoion coincidence spectrometer: case of the amino acids tryptophan and phenylalanine

François Gaie-Levrel,*[a] Gustavo A. Garcia,[a] Martin Schwell[b] and Laurent Nahon[a]

Received 6th December 2010, Accepted 10th February 2011
DOI: 10.1039/c0cp02798g

Gas phase studies of biological molecules provide structural and dynamical information on isolated systems. The lack of inter- or intra-molecular interactions facilitates the interpretation of the experimental results through theoretical calculations, and constitutes an informative complement to the condensed phase. However advances in the field are partially hindered by the difficulty of vaporising these systems, most of which are thermally unstable. In this work we present a newly developed aerosol mass thermodesorption setup, which has been coupled to a Velocity Map Imaging (VMI) analyzer operated in coincidence with a Wiley–McLaren Time of Flight spectrometer, using synchrotron radiation as a single photon ionization source. Although it has been previously demonstrated that thermolabile molecules such as amino acids can be produced intact by the aerosol vaporisation technique, we show how its non-trivial coupling to a VMI analyzer plus the use of electron/ion coincidences greatly improves the concept in terms of the amount of spectroscopic and dynamic information that can be extracted. In this manner, we report on the valence shell ionization of two amino acids, tryptophan and phenylalanine, for which threshold photoelectron spectra have been recorded within the first 3 eV above the first ionization energy using synchrotron radiation emitted from the DESIRS beamline located at SOLEIL in France. Their adiabatic ionization energies (IEs) have been measured at 7.40 ± 0.05 and 8.65 ± 0.02 eV, respectively, and their spectra analyzed using existing theoretical data from the literature. The IE values agree well with previously published ones, but are given here with a considerably reduced uncertainty by up to a factor of 5. The photostability of both amino acids is also described in detail, through the measurement of the state-selected fragmentation pathways *via* the use of threshold electron/ion coincidences (TPEPICO), with appearance energies for the different photofragments given for the vaporization temperatures studied, in correlation with the different molecular orbitals involved as identified from the Threshold Photoelectron Spectra (TPES).

Introduction

The study of fragile biomolecules in the gas phase is still a challenge in experimental physical chemistry. Not only is their volatility extremely low but also they can easily undergo chemical degradation when being heated. However, such studies are of utmost importance if one wants to measure directly the intrinsic physico-chemical properties of these species, which is of considerable interest in life sciences. Gas phase studies bring complementary information to those obtained by most condensed-phase techniques (X-ray crystallography or NMR) since they assess the gas phase chemical structure including conformers, electronic structure, and the photostability and dynamics of those systems.[1] Studying biomolecules in detail in the gas phase helps to mimic larger sub-structures of biopolymers. This so-called biomimetic concept is also important for quantum chemistry: the exact determination of intrinsic properties of small biological units isolated from their natural environment permits the modelling of larger biomolecular systems.[2] Furthermore, the gas phase can be directly relevant to *in vivo* conditions when one considers hydrophobic media.[1]

[a] *DESIRS beamline, Synchrotron SOLEIL, L'Orme des Merisiers, St Aubin 91192 Gif-sur-Yvette Cedex, France. E-mail: francois.gaie-levrel@synchrotron-soleil.fr*
[b] *Laboratoire Interuniversitaire des Système Atmosphériques, UMR CNRS 7583, Université Paris Est Créteil et Université Paris Diderot, Institut Pierre Simon Laplace, 61 av. du Général de Gaulle, 94010 Créteil Cedex, France*

In addition, the astrobiology and astrochemistry community is very much interested in photostability of prebiotic molecules such as nucleosides, oligopeptides or amino acids, in order to understand or predict their abundances and survival conditions in different geophysical media, like the interstellar medium or planetary environments.[3] In this particular context, UV irradiation experiments of small biomolecules have been performed using condensed phase samples and lamps with broad spectral emission,[4] as well as tunable synchrotron radiation (SR) based experiments with gaseous samples.[5,6] These experiments have shown for instance that amino acids are more destroyed by VUV radiation-induced dissociative ionization than nucleobases.[6] Considering the biological importance of amino acids, a better understanding of their interactions and chemical reactivity needs precise knowledge of their valence-shell ionic electronic structure which can be probed, for example, by photoelectron spectroscopy (PES).[7,8]

There is therefore a growing scientific need for experimental methods to transport fragile biomolecules into the gas phase. Vaporization/ionization methods, such as Electro-Spray Ionization (ESI)[9] or matrix assisted laser desorption ionization (MALDI),[10] have been used for this purpose, often coupled to mass spectrometry as it has been done for Trp and Phe.[11,12] They are labelled "soft vaporization" because, when proper experimental conditions are applied, intact molecular ions can be produced with minimal fragmentation. However, biomolecules are released as multicharged ions from small charged droplets in the ESI process, and as singly- and multiply-charged ions in the MALDI process, so that the spectroscopy and photon-induced processes involving neutral species cannot be assessed.

Laser desorption methods have also been successfully applied to the propagation of *neutral* biomolecules to the gas phase.[13] The disadvantage of this method is the low repetition rate of the desorption laser which is not compatible with continuous probe sources such as SR and the use of coincidence techniques. Furthermore, laser instabilities may lead to unstable experimental conditions making difficult the acquisition of quantitative spectroscopic data. In addition, the produced molecules may be quite strongly heated in the laser-desorption process leading to the production of a large tautomer distribution.[14]

Other vaporization techniques were developed quite independently by the atmospheric aerosol community. Because of the need to measure in real time, at the molecular level, the composition of atmospheric aerosols, several types of so-called aerosol mass spectrometers (AMS) have been developed. As recently reviewed,[15] different vaporization/ionization schemes have been applied as laser desorption/ionization (LDI) for example.[16,17] One way to overcome molecular fragmentation involved in the LDI process is to use a two-step desorption/ionization scheme: here, vaporization is generally accomplished by using either a pulsed infrared laser, at $\lambda = 10.6$ μm,[16,18] or by flash-vaporization on a heated surface (thermal desorption process).[16,19] Both techniques leave the desorbing neutral molecules intact and can therefore be qualified as "soft". The ionization step can be performed using Resonant 2 Photon Ionization (R2PI)[16] or Single Photon Ionization (SPI). SPI is achieved by using VUV laser radiation,[20] VUV lamps,[21,22] as well as VUV-SR.[23–26] Wilson *et al.*[25,26] have combined aerosol thermal desorption with SR-based Time-of-Flight (TOF) mass spectroscopy to record total ion yields from fragment-free biomolecules, from which adiabatic ionization energies can be determined taking advantage of the tunability of VUV-SR. However, their experiment does not measure the electron's energy, so that the amount of internal energy deposited into the ion is not known, nor the ionic states spectroscopy.

The use of electron/ion coincidence schemes, especially operating in the threshold photoelectron–photoion (TPEPICO) mode, is able to provide accurate ionization energies, a detailed analysis of the ion electronic structure, richer than a simple integrated ion current, as well as fragment appearance energies from a state-selected parent ion. Therefore, in this paper, we present an aerosol source paired with flash-vaporization on a heated surface (called the thermodesorber (TD) in the following) coupled to an existing Velocity Map Imaging (VMI)/Wiley–McLaren TOF (WM-TOF) electron/ion coincidence spectrometer called DELICIOUS II.[27] To our knowledge, this is the first time an aerosol thermodesorption source is coupled to an electron spectrometer in general and to a VMI coincidence spectrometer in particular, overcoming the difficulties of inserting a TD inside the VMI's inhomogeneous electric field. We are thus able to benefit from the known advantages of a VMI spectrometer,[28] namely the possibility of recording simultaneously the electron's kinetic energy with high resolution, the angle of its ejection and the ability to detect threshold photoelectrons with sub-meV resolutions.[27] In addition, photoelectron images are recorded in coincidence with a specific mass, providing PhotoElectron PhotoIon COincidence (PEPICO), or Threshold-PEPICO (TPEPICO) measurements.

This experiment, connected to the VUV DESIRS beamline,[29] at the French 3rd generation synchrotron facility SOLEIL, possesses a manifold scientific case:

(1) The unravelling of the thermochemistry of thermolabile biomolecules by recording their ionization and fragmentation footprints *via* threshold photoionization spectroscopy (TPEPICO) at high resolution.

(2) The chiroptical properties study of gas phase pure enantiomers of biomolecules and especially their photoelectron circular dichroism (PECD)[30] in connection with a possible link to the origin of life's homochirality.[31] The case of homochiral nanoparticles can also be investigated, with expected amplified PECD because of crystallization effects.

(3) The measurement of the composition of chemically complex particles, like those of atmospheric interest such as secondary organic aerosols produced in a smog chamber.

In the following sections we will introduce the performances of the experimental apparatus, and then focus on the first topic that has been adressed with this setup, namely the photoionization of the two amino acids, Trp and Phe, for which the TPEPICO spectra have been recorded in the region of the first few eV's above the valence ionization thresholds. The results will be discussed in connection with earlier measurements, in order to highlight the capabilities of the current setup.

1. Experimental setup and methodology

Tryptophan and phenylalanine nanoparticles were produced by nebulising solutions of 1 g L^{-1} in water of both commercially available amino acids (Sigma Aldrich, >99% purity) using a constant output atomizer (TSI model 3076) followed by a diffusion dryer (TSI model 3062). Our instrument is based on three components (Fig. 1): (1) an aerodynamic lens system integrated in the SAPHIRS molecular beam chamber,[32] sampling the nanoparticles and producing a highly collimated beam, (2) an optical detection unit is employed to detect the scattered light of the particle beam in order to align and characterize the aerosol beam, and to monitor the stability of the source, and (3) a thermodesorber (TD), inserted between the extraction plates of the VMI/WM-TOF spectrometer to continuously vaporize the nanoparticles of the beam. Neutral molecules of the resulting vapour plume are then ionized by the VUV-SR.

1.1 Aerodynamic lens system and optical detection

The aerodynamic lens system was designed by using the McMurry's group model[33] and consists of eight precision-machined orifice lenses, all mounted in a 17 mm internal diameter (id) precision stainless steel tube and starting from 4 mm at the inlet and gradually decreasing to 3 mm at the exit, all held in position by spacers. The entrance of the lens system is formed by a 160 μm id orifice, which fixes the gas flow rate inside the system to about 0.15 L min^{-1}, followed by a 9 cm relaxation chamber upstream of the first lens. This lens system focuses the particles onto a central axis and the final exit aperture—the accelerating nozzle—controls gas expansion and particle acceleration into the vacuum system. The lens tube is mounted in the SAPHIRS expansion chamber, on a XYZ translation stage (precision = 10 μm), and is aligned with the center of the 1 mm skimmer joining the expansion and ionization chambers. Two 1000 L s^{-1} turbomolecular pumps (Seiko, model STPH1000C) are used to evacuate this chamber and maintain the flow through the lens. When the inlet of the lens system is open, the pressure inside the expansion chamber is $\sim 1 \times 10^{-3}$ mbar.

The performances of the aerodynamic lens system have been modelled using the software described in ref. 33. The transmission efficiency is about 100% for particle diameters ranging from 100 nm up to 1.5 μm. The modelled particle beam diameter, 10 cm downstream the outlet of the lens system, *i.e.* at the vertical axis of the DELICIOUS II spectrometer (see Fig. 1), is less than 0.35 mm and the average velocity of the particles is about 115 m s^{-1}.

An optical detection unit is employed to detect the Mie scattered light of the particles. This optical detection is composed of a continuous diode-pumped solid-state laser (Shanghai Dream Lasers Technology Co., Ltd.) operating at 532 nm and precisely aligned in the horizontal plane, perpendicularly to the skimmer axis. The measured laser beam waist diameter is 250 μm and the distance between the laser beam and the tip of the skimmer is 5 ± 1 mm. A photomultiplier tube (model XP311002/02, Photonis) detects the scattered light of the particles at an angle of 90° with respect to the laser propagation axis.

The experimental characterization of the aerosol beam diameter was done using this optical setup with dioctylphthalate (DOP) particles. The aerodynamic lens system was scanned along the vertical axis in front of the CW laser. The z distance $d_{lens\_out/laser}$ between the outlet of the lens system and the laser beam was fixed to 20 ± 1 mm. The scan provided a Gaussian shape signal with a full width at half maximum (FWHM) of 350 μm after deconvolution of the laser beam diameter, in very good agreement with theoretical expectations. At $d_{lens\_out/laser}$ = 70 ± 1 mm, the experimental deconvoluted FWHM of the nanoparticles beam is 400 μm. From these two measurements we estimated the total divergence of the particle beam at just 1 mrad.

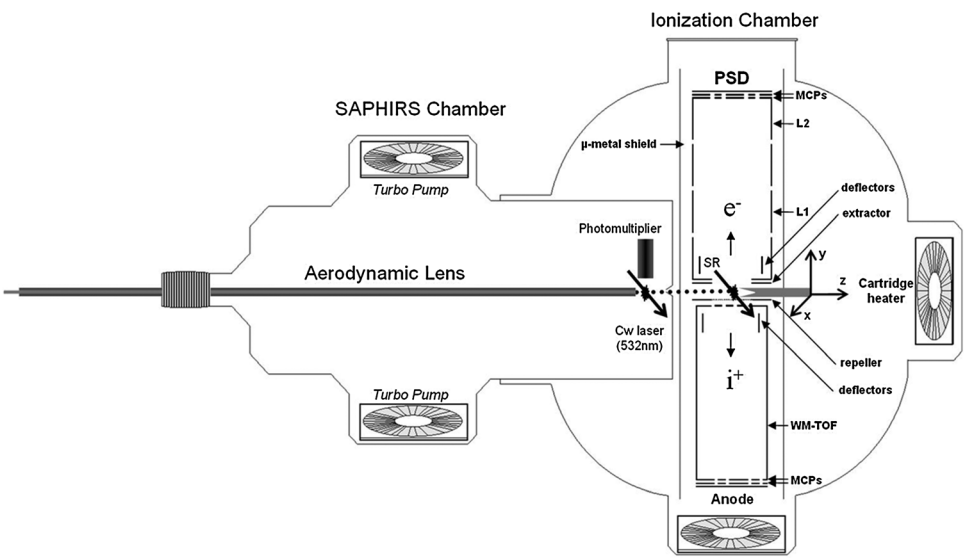

Fig. 1 The new aerosol source implemented in the SAPHIRS versatile molecular beam chamber composed of three parts: (1) an aerodynamic lens system, (2) an optical detection unit, (3) a thermal desorption module inserted in the ionization region of a PEPICO spectrometer.

1.2 Aerosol thermodesorption coupled to an imaging photoelectron/photoion coincidence spectrometer

After passage of the skimmer, the nanoparticles arrive inside the ionization region where they are thermally vaporized and photoionized. The z distance between the skimmer tip and the spectrometer vertical axis is 8 cm. The ionization chamber is pumped by one 1000 L s^{-1} (Leybold, TurboVac 1000) and one 70 L s^{-1} turbo molecular pump (Varian V-70LP) to reach 10^{-6} mbar when the lens inlet is open. The photoions and photoelectrons are produced at the center of the DELICIOUS II spectrometer which is described in detail elsewhere.[27] Briefly, after being accelerated in opposite directions, electrons and ions enter a VMI and a WM-TOF analyzer respectively, where they are detected in coincidence. The spectrometer is capable of recording threshold photoelectrons with sub-meV resolution, or fast electrons (up to 17 eV kinetic energy) with a 5% energy resolution. The ion mass resolution is around 150 when operated with a molecular beam.

The alignment between the aerosol beam and the ionization region is performed by scanning the aerosol beam in the xy plane—the skimmer being mechanically centered with respect to the ionization region—and measuring the total photoelectron yield produced by the nanoparticles photoionization only, *i.e.* with the TD extracted. As an example, a ±1 mm xy-2D map obtained for a beam of tryptophan nanoparticles at 8.5 eV with 100 μm steps and a 1 mm skimmer is shown in Fig. 2. The purple square at the center indicates the optimized position of the aerodynamic lens system. Note that the vertical footprint corresponds to a convolution between the aerosol and photon beam sizes (~210 μm with a 200 μm exit slit), while the horizontal footprint is a convolution of the skimmer (1 mm) and the aerosol beam sizes, which explains why the image is narrower along the y-axis.

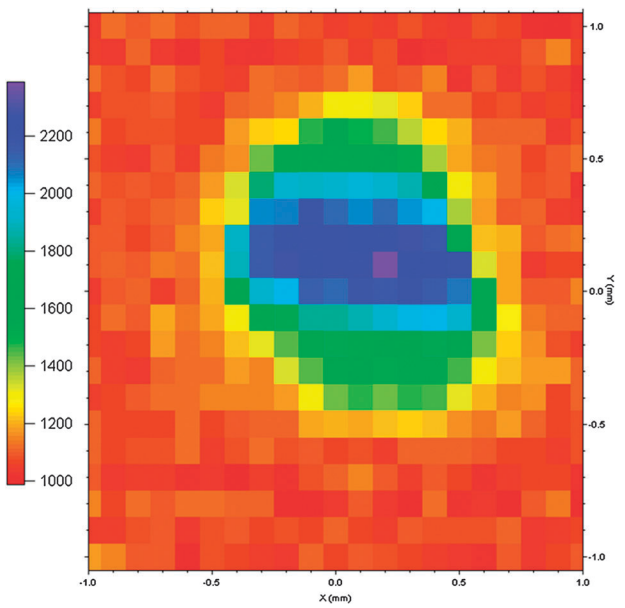

Fig. 2 2D jet mapping at 8.5 eV of the aerodynamic lens system through a 1 mm skimmer. This grid represents the electrons count signal as given by the linear color scale, obtained from the photoionization of tryptophan nanoparticles without thermal desorption and corresponds to a ±1 mm displacement of the lens system along its X and Y axes with 100 μm steps. The purple square represents the maximum signal and, therefore, the optimized position.

The custom-built TD module is located downstream of the aerosol beam, in the middle of the extraction plates of the spectrometer. It consists of a 70 mm rod of porous tungsten, ~20% void volume with pore sizes of ~100–200 μm, whose front section (where the particles impact) has an inverted cone shape with a 90° angle. Both the cone shape and the porosity were chosen to reduce the bouncing effect of the particles. The TD is mechanically maintained onto a copper body containing a 6.5 mm-diameter cartridge heater (Watlow Electric) driven by a power controller. The cartridge heater temperature is measured with an internal thermocouple and can be adjusted up to 870 K. A specific calibration was performed with a second thermocouple inserted inside the tip (under vacuum), in order to precisely know the temperature at the cone-shaped TD tip, which is the temperature we will refer to in the following. The TD module is maintained by a XYZ translation stage allowing the optimization of its position with respect to the aerosol beam and the SR axis.

The dimensions of the TD were optimized through ray-tracing simulations performed with the Charged Particle Optics 3D (CPO-3D) software (Scientific Instrument Services, Inc.). This step was crucial to determine the maximum diameter of the TD that can be inserted inside the spectrometer ionization source without distorting the VMI focalization field. It was found that a TD diameter of 3 mm led to satisfactory results down to a distance $d_{TD/SR}$ (in the z direction) between the TD and the ionization volume of about 3 mm, and that a bias voltage had to be applied to the TD to correct its effect on the electric field. In practice, we were able to insert the TD down to $d_{TD/SR}$ = 1 mm from the SR axis while keeping a high quality image. The applied voltage on the TD depends on the distance $d_{TD/SR}$. For $d_{TD/SR}$ = 13 mm, a voltage of V_{TD} = 0.88 × V_{rep} is needed, while for $d_{TD/SR}$ = 1 mm, a lower value of V_{TD} = 0.80 × V_{rep} is applied, where V_{rep} represents the potential on the repeller electrode.

Fig. 3(A) shows, in the later conditions ($d_{TD/SR}$ = 1 mm), a raw photoelectron coincidence image of Ar obtained at 16 eV. The image exhibits two circular patterns corresponding to the $^2P_{3/2}$ and $^2P_{1/2}$ electronic states of Ar^+ and demonstrates the ability of the spectrometer to record nicely circularly-shaped images with a TD inserted as close as 1 mm from the ionization region. Under the same experimental conditions, and taking advantage of the spectrometer's ability to discriminate spatially the hot electrons,[27] Fig. 3(B) shows a Threshold PhotoElectron Spectrum (TPES) of the $^2P_{3/2}$ state of Ar obtained in the 15.72–15.80 eV energy region with 1 meV steps and a TD heated at 373 K. The spectrometer extraction field was set to provide a threshold energy resolution of 7 meV, and demonstrates that the quality of the TPES is not affected by the presence of the hot TD.

When a solid or liquid particle impacts on the TD, a neutral molecular cloud is formed, whose spatio-temporal properties are poorly known. According to Sykes *et al.*,[19] it is assumed that the molecular cloud that leaves the heater has some velocity distribution approximated with a Maxwell–Boltzmann distribution which depends on the molecular weight M of the

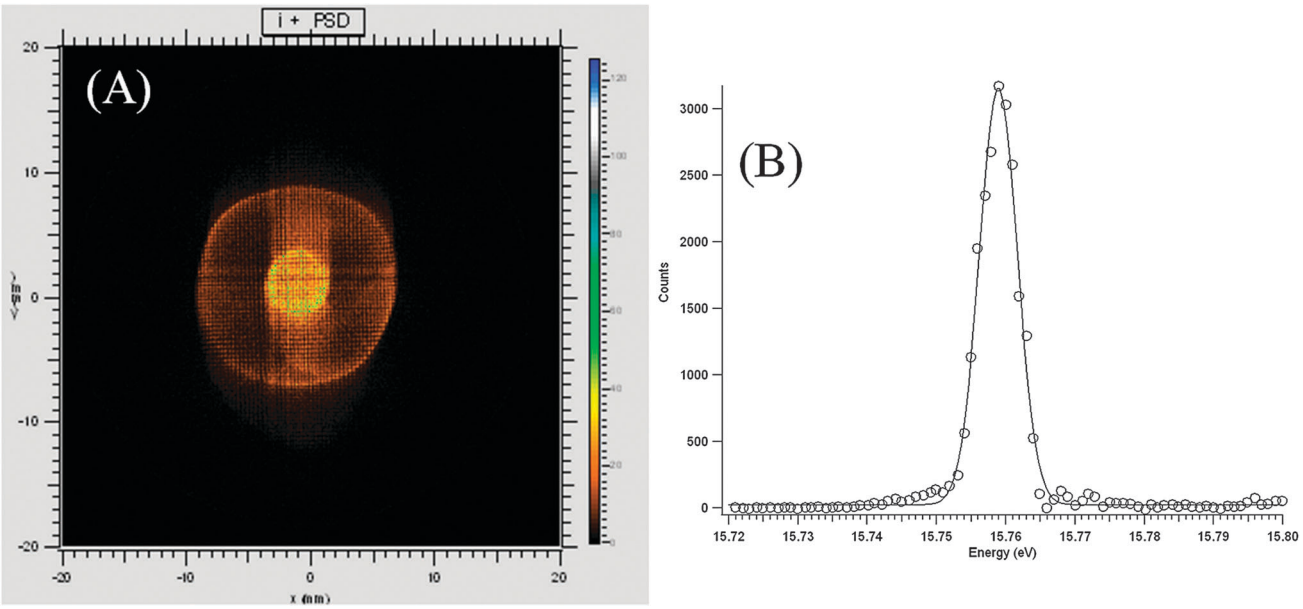

Fig. 3 (A) Raw photoelectron image of Ar obtained in PEPICO mode at 16 eV with $d_{TD/SR}$ = 1 mm. The two circular patterns correspond to the $^2P_{3/2}$ and $^2P_{1/2}$ electronic states of Ar^+; (B) Threshold PhotoElectron Spectra (TPES) of the $^2P_{3/2}$ state of argon between 15.72 and 15.80 eV with 1 meV step obtained with the hot electrically charged thermodesorber (373 K) inserted in the source of the spectrometer with $d_{TD/SR}$ = 1 mm.

considered molecule and the temperature T of the TD. Sykes *et al.*[19] have converted this Maxwell–Boltzmann distribution into a distribution of molecule arrival times at the ionization region, after travelling the distance $d_{TD/SR}$. Applying their procedure and considering M = 200 g mol^{-1}, T = 423 K, $d_{TD/SR}$ = 1 mm, and neglecting the initial impact energy, the mean delay time required for the flash-evaporated gaseous molecule to travel the distance $d_{TD/SR}$ is about 100 μs. A larger $d_{TD/SR}$ results in broader arrival time distribution and an increased divergence angle of the molecular cloud and, therefore, a lower density of molecules in the ionization region. This was experimentally verified by increasing $d_{TD/SR}$, *i.e.* retracting the TD along its Z-axis with fixed X and Y positions, and by recording the ion signal intensity at each translation point with the same acquisition time. As previously reported by Wilson *et al.*,[25] we observed that the ion signal decays as $\sim 1/d_{TD/SR}$. In the following, we will only present data corresponding to a $d_{TD/SR}$ = 1 mm working distance (except for the DOP nanoparticles study described in Section 2.1 for which the TD was fully retracted), which provides a high density of biomolecules allowing the use of first-order monochromatized SR with still satisfactory count rates.

1.3 The VUV synchrotron photon beam

VUV radiation from the DESIRS beamline located at the SOLEIL synchrotron facility was used as the ionizing radiation. This undulator-based[34] beamline delivers tunable energy and variable polarization in the 5 to 40 eV range, and is equipped with a 6.65 m normal incidence monochromator in the Eagle off-plane configuration[35] equipped with four gratings to cover the whole energy range, with a fully adjustable resolution/flux compromise. For experiments presented in this paper we chose the 200 grooves mm^{-1} grating with a resolving power of up to 4000, delivering 10^{12}–10^{13} ph s^{-1} at 0.1% bandwidth. High spectral purity is achieved by means of a gas filter[36] located upstream of the sample, which effectively filters out the contributions from the higher harmonics of the undulator which could be transmitted by the grating. Note that great care was taken at the beamline conception stage to minimize optical aberrations so that the SR footprint (yz plane) is tightly focused with in particular a FWHM in the horizontal direction (z-axis) of 200 μm. This tight focus allows the use of a short $d_{TD/SR}$ (as short as 1 mm) without producing spurious secondary electrons on the TD tip that would be detrimental to the data quality.

2. Results and discussion

The experiments presented in this paper concern mainly the amino acids Trp and Phe which have been chosen both for their biological relevance, and because they have already been studied by various groups[25,37,38] so that a comparative evaluation of the experimental performances is possible. Before, we also present the results obtained with dioctylphthalate nanoparticles. DOP, a viscous oil, is widely employed by the atmospheric aerosol community as a benchmark for testing and calibration purposes of aerosol instrumentation since it can be nebulized easily and provides a constant stream of particles.

2.1 Photon-induced processes on DOP nanoparticles

Accurate operation of this new instrumentation was first investigated with DOP particles (parent ion: m/z 390), as described in Section 1.1, *without* the TD module in order to study photon-induced processes on the nanoparticles themselves. Fig. 4 shows a Threshold Photoelectron Spectrum (TPES) of the DOP nanoparticles (triangles) obtained

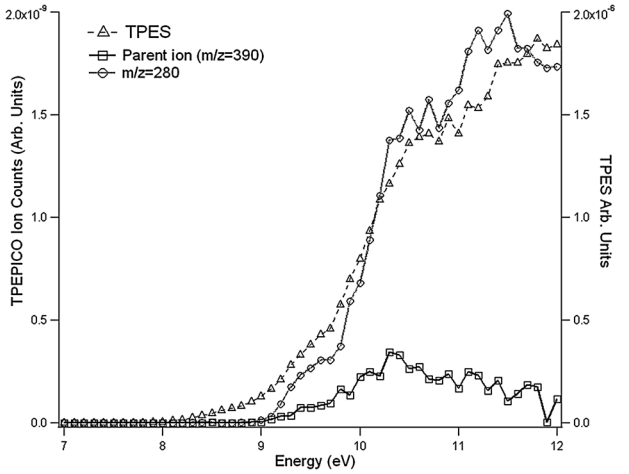

Fig. 4 Threshold Photoelectron Spectra (TPES) of DOP particles obtained without coincidences between photoelectrons and photoions (triangles) and with a 300 meV electron resolution; TPEPICO spectra for the ions m/z = 390 and m/z = 280 (circles and squares). These three spectra were obtained without the thermal desorption module.

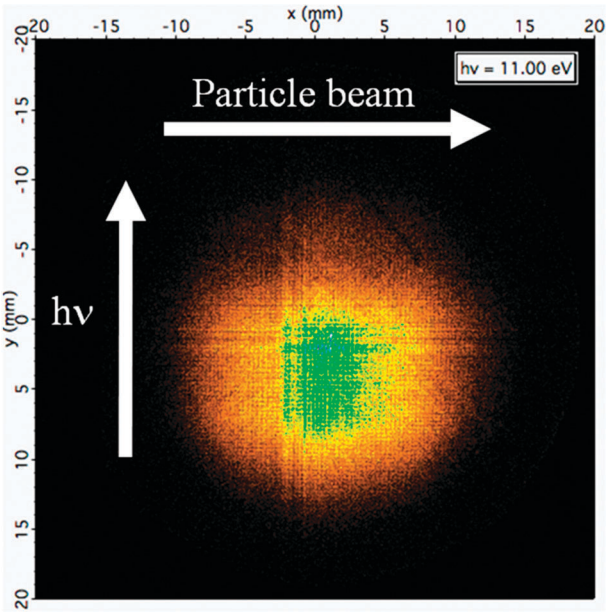

Fig. 5 Photoelectron image of polydisperse homogeneous DOP particles recorded at a photon energy of 11 eV. Arrows indicate the propagation direction of the particle beam and synchrotron radiation ($h\nu$).

with a 300 meV and 1 meV electron and photon resolution, respectively. Due to the volatility of DOP and the high concentration of DOP particles in the aerosol beam and therefore in the ionization chamber, it was possible to detect also the gas phase parent ion at m/z 390 as well as its major fragment at m/z 280 even though the TD was not inserted into the ion source during this experiment. It is interesting to present the PEPICO spectra of the parent and fragment cations in the same Fig. 4 (squares and circles respectively). Comparing the nanophase TPES with the monomer PEPICO spectrum, we observe that the ionization of the former starts as low as 8 eV while the gas phase species ionization onset appears around 9 eV. Therefore, the ionization energy of nanophase DOP appears to be shifted by about 1 eV to lower energies with respect to the monomer and its major fragment. Such a lowering of the ionization energy, a well-known phenomena in van der Waals clusters, has been observed in nanophase glycine too with a 1.7 ± 0.2 eV shift that was explained in terms of intermolecular polarization in the molecular crystal of the nanophase, a consequence of aggregation.[26] The nanoparticle cation complex is thermodynamically more stable than the monomer, due to charge delocalization. The long tail from 8 to 9 eV could be due to the polydisperse nature of the particles coming from the atomizer, since they are not size-selected.

The angular distribution of photoelectrons emitted from polydispersed homogeneous DOP particles was also recorded during this experiment. Fig. 5 shows a photoelectron image obtained at a photon energy of 11 eV. Arrows indicate the propagation direction of the particle beam and synchrotron radiation. There is a clear shadowing of photoelectron intensity emanating at the opposite side of the particle beam illuminated by the incoming SR. As discussed by Wilson *et al.* in the case of NaCl nanoparticles,[39] the produced photoelectron angular pattern is largely due to the internal electric field distribution inside the particle. They also showed that the asymmetry in photoemission arises because both the photon penetration depth and electron escape length are comparable to the diameter of the particle.

2.2 VUV ionization of thermally desorbed tryptophan molecules

Fig. 6 shows the PEPICO mass spectra of Trp obtained at 8, 9 and 10.5 eV, with the TD inserted at a distance $d_{TD/SR}$ = 1 mm from the ionization region and heated to 373 K (Fig. 7A), 423 K (Fig. 7B) and 553 K (Fig. 7C). Due to the larger size of the volume source during the thermodesorption process, the increase Doppler speed distribution of the neutral molecules as compared to a molecular beam, and the presence of the TD which induces the inhomogeneous field inside the spectrometer source because of the optimization for the electron image, a mass resolution lower than 150 is observed, which is nevertheless sufficient for the present scientific purpose. For the detection of light species elimination channels, one would compromise the quality of the electron image in favour of mass resolution by changing the potential applied to the TD.

The mass spectra obtained at 8 eV are fragment-free at 373 and 423 K. In all other spectra, the main Trp fragment, the methylene indole cation at m/z 130, is present too. As it is expected, for a fixed temperature, the fragment m/z 130 starts appearing with increasing photon energy because of dissociative ionization processes. In this series of mass spectra the m/z 130 fragment starts to be discernible at 9 eV and T_{TD} = 373 K. On the other hand, for a fixed photon energy, the fragment (m/z 130) to parent (m/z 204) ratio (F/P) is also increasing when the vaporization temperature increases. For example, at 9 eV the F/P ratios are 0.3 and 3.6 at 373 and 553 K respectively. Our results on F/P ratios at various temperatures and photon energy are in good agreement with the work of

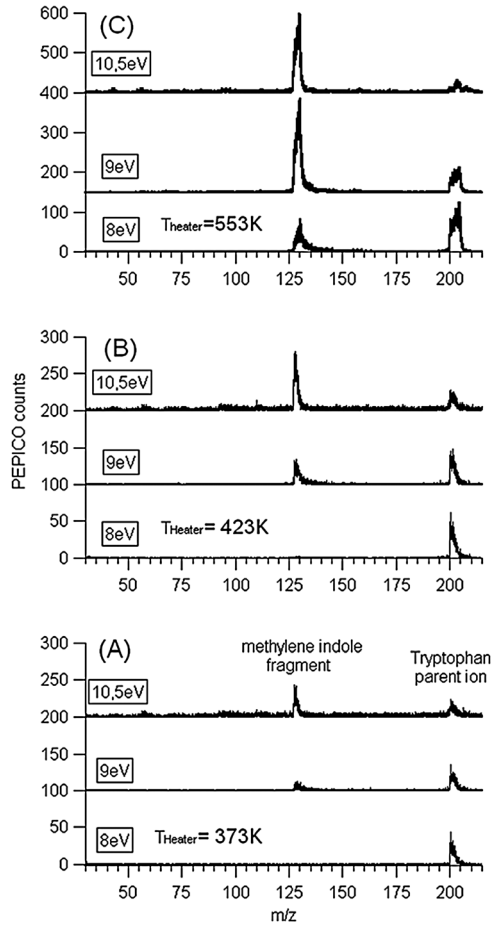

Fig. 6 PEPICO mass spectra of tryptophan obtained at 8, 9 and 10.5 eV at three temperatures: (A) 373 K, (B) 423 K, (C) 553 K.

Wilson *et al.*,[25] with only slight differences. For example, at 8 eV and 373 K, Wilson *et al.*[25] obtained a F/P ratio of 0.04 whereas under these conditions, our spectrum is totally fragment free. This group also observed an exponentially increasing F/P ratio with rising temperature (at fixed photon energy). This "Arrhenius like" behavior suggests the existence of an activation barrier that leads to an extensive fragmentation during the photoionization process when the neutral molecule is thermally activated. In other words, at a fixed photon energy, Trp dissociates from the hot ground state of the ion when the heater temperature is rather high. Therefore, by controlling the vaporization temperature and photon energy, it is possible to control the molecular fragmentation of the studied compounds. Interestingly, even at 553 K and at 10.5 eV, we do not observe the second fragmentation channel leading to a m/z 116 fragment (indole ion) that is reported by Wilson *et al.*[25] at 573 K above $\sim$7.5 eV. This means that the temperature onset for the appearance of this fragment is quite sharp, located between 553 and 573 K.

The tryptophan ionization energy has been measured *via* several gas phase experiments performed in the last decades. By photoelectron spectroscopy, Seki and Inokuchi and Campbell *et al.* determined the Trp ionization energy to be, respectively, 7.3 $\pm$ 0.1 eV[40] and 7.2 $\pm$ 0.2 eV.[41] More recently, Wilson *et al.*[25] determined the tryptophan ionization energy to be 7.3 $\pm$ 0.2 eV by using SR-mass spectrometry coupled to an aerosol thermal desorption module to vaporize tryptophan nanoparticles. These authors were not able to determine more accurately this ionization onset due to the bandwidth of their undulator radiation, directly transmitted to the sample *via* the zeroth order of the monochromator's grating, and also because of the inability of their undulator to get to energies below 7.2 eV.

Fig. 7 shows TPEPICO spectra of the tryptophan parent ion (m/z 204) and its major fragment (m/z 130) obtained in the present work. The red and blue shaded areas correspond to the errors bars which result from a Poisson distribution applied to the ion counts on the respective mass peaks. Fig. 7(A) was recorded between 7 and 10 eV at 423 K with a 17 meV photon resolution (53 meV total resolution). From the TPEPICO curves, the adiabatic ionization energy of the m/z 204 ion is determined at 7.40 $\pm$ 0.05 eV (see the onset close-up in Fig. 7(B)) by linear extrapolation of the onset. This value is in good agreement with the previously reported values, but we were able to lower the uncertainty to 50 meV due to the high thermodesorption signal, which enabled us to work with monochromatic light (1st order of the monochromator) and to use the electron/ion coincidences to state-select the ions with a high resolution. We have limited ourselves to 50 meV threshold energy resolution since in the case of these large potentially floppy molecular systems, the state density and the presence of several conformers combine to produce a poorly structured TPEPICO spectrum, at least for the two molecules under study here. From Fig. 7(A), we can observe that the methylene indole fragment (m/z 130), produced by the Cα–Cβ bond breaking, has an appearance energy $\sim$0.5 eV higher than the parent ion (m/z 204) onset at this temperature.

Fig. 7(C) shows TPEPICO spectra of the two Trp ions between 7 and 10 eV at a higher temperature, at 558 K, and with a much lower total resolution of 300 meV. The parent ion onset is unchanged compared to the 423 K spectrum, in agreement with current understanding and literature (see for example the review by Genuit and Nibbering[42]). In other words the temperature effect is not visible as hot bands in the neutral (because of unfavourable Franck–Condon factors) that would produce a long-wavelength tail on the parent TPEPICO curve, but is rather reflected in the ion hot ground state which in turn fragments. Indeed, by comparing both spectra obtained at 423 and 558 K, we can clearly observe a difference in the AE of the m/z 130 fragment, in line with our precedent discussion on the F/P ratio. To date, we are only able to give AEs as the first rising point of the onset of the TPEPICO curves. Thus, with thermodesorber temperatures of 423 and 558 K, methylene indole AEs are estimated to be 7.99 $\pm$ 0.05 and 7.42 $\pm$ 0.05 eV, respectively. Therefore, at 558 K, the methylene indole fragment AE is lower by 0.57 $\pm$ 0.1 eV than at 423 K. The methylene indole 0 K AE value will be determined in a forthcoming paper by comparing our breakdown diagrams obtained from TPEPICO spectra to the data obtained from a data analysis computer code[43] capable of modelling a wide variety of dissociation mechanisms.

Perfectly consistent with our results, Wilson *et al.*[25] also determined a shift of 0.5 eV for the m/z 130 AE, when going from 373 to 573 K. They performed frequency calculations to

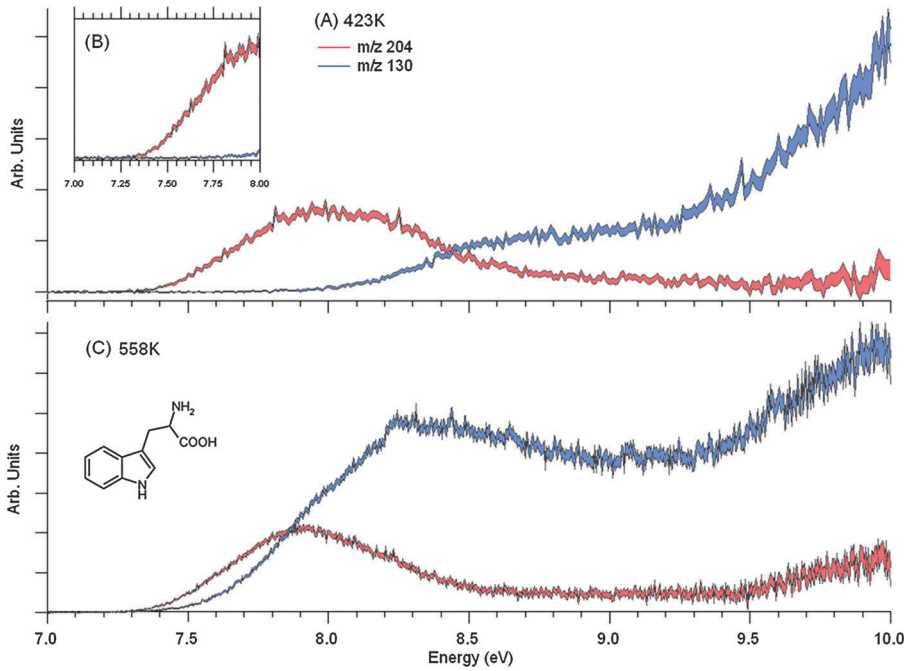

Fig. 7 TPEPICO spectra of the tryptophan parent ion (m/z = 204) and its major fragment (m/z = 130) (A) between 7 and 10 eV at 423 K with a 50 meV electron resolution and a 17 meV photon bandwidth, (B) close up of the (A) spectra between 7 and 8 eV, (C) between 7 and 10 eV at 558 K with a 300 meV electron resolution.

compute the internal energy change of Trp for this temperature rise and found a value of 0.62 eV, thus of similar order of magnitude than the experimentally observed shift. This shift is therefore mainly due to the internal/thermal energy imparted to the neutral molecule during the vaporization process.

High resolution TPES spectra of biomolecular species, recorded close to the ionization threshold, can be compared to theoretical calculations of the ionization energies of different conformers. In principle, this could reveal the conformer distribution present in the gas phase for a given temperature. These kinds of calculations are of particular interest to our measurement technique because we are able to precisely control the internal energy content of the formed ions. Dehareng and Dive[44] have calculated vertical ionization energies of α-amino acid conformers considering three types of backbone conformations of the R–C(NH_2)H–COOH molecular unit (CF1, CF2, CF3). They used the Outer Valence Green's Function (OVGF) approximation available in the Gaussian program package and further considered different orientations of side chains R.

For neutral Trp, three energetically low-lying conformers are identified by geometry optimization. They correspond to two stable backbone conformations, CF1 and CF2(1), and a third one, CF2(2), with the same backbone conformation but another side chain orientation. Vertical IEs are then calculated in the OVGF framework. They have also described all occupied valence molecular orbitals (and an equal number of virtual MOs) with a description of the ionized MOs at the Restricted Hartree Fock (RHF) level. Fig. 8 shows our experimental Threshold Photoelectron Spectrum (TPES, blue curve), derived from the TPEPICO spectrum presented in Fig. 7(A), with a total resolution of 53 meV, together with calculated ionization energies according to ref. 44 as given by the black (CF1), green (CF2(1)) and red (CF2(2)) sticks for the three conformers. The intensity ratio of the sticks is inferred from a calculated Boltzmann distribution of the conformers at 423 K, knowing their calculated relative energies at the B3LYP level (Table 1 in ref. 44). The red curve is a Gaussian convolution of the stick diagram taking into account our 53 meV spectral resolution as FWHM. In this energy range, four molecular orbitals can be ionized. In the onset region, Trp has aromatic π-orbitals with lower ionization energy than the non-binding n_N and n_O orbital contribution of the amino and carboxylic groups which are located in the 9.4–9.8 energy range. By comparison with Fig. 7(A), the removal of an electron from the two π-orbitals does not seem to trigger the fragmentation toward methyl-indole as they leave the parent ion intact.

The second rise of the TPES curve, starting at approximately 9.3 eV, is likely to concern five molecular orbitals which can be described as lone-pair, π-like and σ orbitals for the three related conformers. In this region the breaking of the C_α–C_β bond to produce the methyl-indole fragment is much more favourable and at 10.0 eV, around the Lymann-α, it is the only ion present within the error bars, the parent ion being completely dissociated.

The "structureless" shape of our TPEPICO spectra is probably due to the presence of slow vibrational progressions for each of the conformers, hinting at a geometrical rearrangement in the ion following the ionization. Unfortunately, this lack of structure combined with the poor theoretical precision, precludes a detailed elaboration on the conformer population. Indeed, for the most stable conformer of tryptophan, the difference in the predicted first ionization energy between

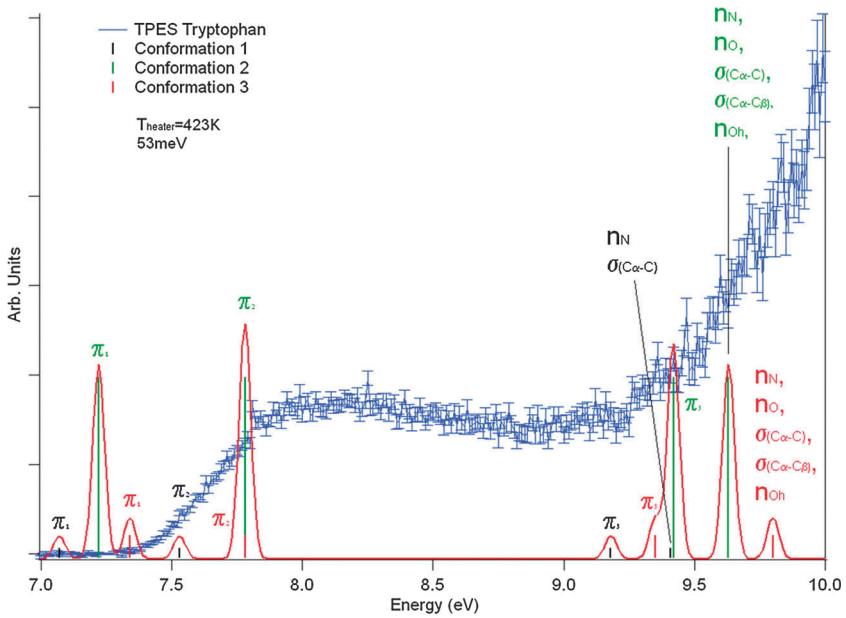

Fig. 8 TPES of tryptophan with a total resolution of 53 meV (blue curve); the black, green and red stick diagrams are extracted from OVGF calculations of the three most stable tryptophan conformers (see text): Conformation 1 = CF1, Conformation 2 = CF2(1), Conformation 3 = CF2(2);[47] the red curve corresponds to the convolution between the stick diagram and our total spectral resolution.

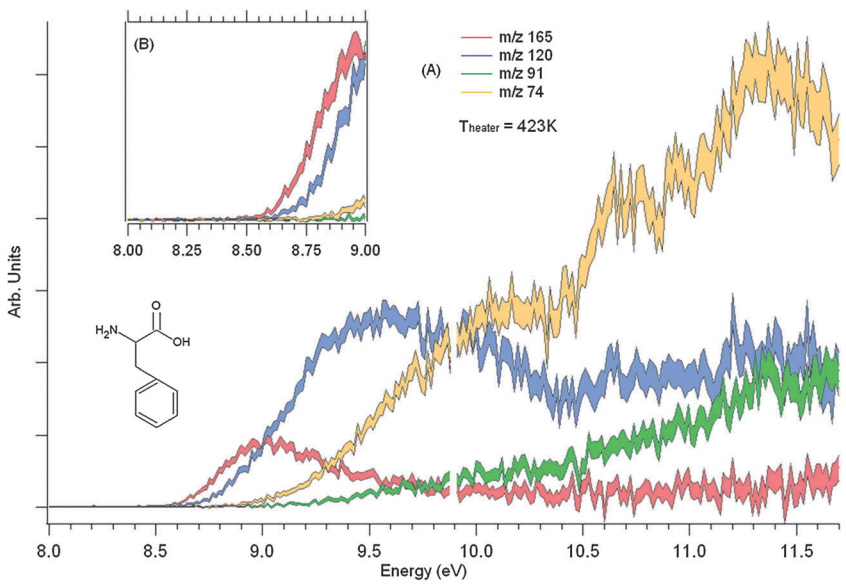

Fig. 9 TPEPICO spectrum of the phenylalanine parent ion (m/z = 165) and its major fragments (m/z = 120; 91 and 74) (A) between 8 and 11.7 eV at 423 K with a 20 meV electron resolution and a 17 meV photon bandwidth, (B) close up of the (A).

OVGF and MP2 methods reaches 0.6 eV. However, this has to be verified in the future with measurements at even higher resolution and TPES simulations using quantum chemical calculations of conformer dependent Franck–Condon factors (FCFs).

2.3 VUV ionization of thermally desorbed phenylalanine molecules

Even if Phe was less studied than Trp, its photoionization has been investigated by PES[41,45] and R2PI.[38,46] Campbell *et al.* determined its adiabatic IE to be 8.5 ± 0.2 eV.[45] This value is in good agreement, within the error bars, with the one obtained *via* ion yield by Wilson *et al.*[25] at 523 K, *i.e.* 8.6 ± 0.1 eV. The TPEPICO spectrum of phenylalanine obtained in this work is plotted in Fig. 9(A) showing the parent ion (m/z 165) and its major fragments (m/z 120; 91 and 74) between 8 and 11.7 eV at 423 K with a 20 meV electron resolution and a total resolution of 27 meV. A close-up of the parent ion onset is presented in the (B) panel of Fig. 9, between 8 and 9 eV. By using the same method as used for Trp, we determined the adiabatic ionization energy of phenylalanine to be 8.63 ± 0.02 eV, which is consistent with previously published values, but is given here with a five-fold decrease

of the uncertainty in the absolute energy determination. We can notice that, at 423 K, the appearance energy of the m/z 120 ion, which is the lowest of the three fragment ions considered here, is very close to the ionization energy. By analogy with the temperature dependent Trp measurements, we can infer that the energy difference between Phe^+ and its fragments $(\varnothing\text{–}CH_2CHNH_2)^+ + COOH$ formed by dissociative ionization is probably very low. Note also that the lowest energy ionic fragmentation pathway of Phe is related to the rupture of the Cα-carboxyl bond, in contrast to Trp.

As for the Trp experiment, we are able to give AEs as the first rising point of the onset of the TPEPICO curves. Thus, with a thermodesorber temperature of 423 K, the AEs of the fragments m/z 120, 91 and 74 are estimated to be 8.65 ± 0.02, 9.31 ± 0.02 and 8.95 ± 0.02 eV respectively. These AE values have never been determined before. These TPEPICO spectra will be more precisely interpreted using an elaborated theoretical model[43] in a forthcoming paper, in order to derive precise 0 K appearance energies for all the fragments, taking into account, among other factors, the parent ion's internal energy. For now, the temperature dependence of the AE of the major fragments can be inferred from the PEPICO mass spectra presented in Fig. 10 recorded at 8.8, 9.5, 10 and 10.5 eV for 423 and 473 K TD temperatures. Indeed, at 9.5 eV, F/P ratios for the m/z 120 and 74 fragments at 423 K are 0.5 and 0.1, respectively. These ratios are 2.5 and 1.7 at 473 K, *i.e.*, only by adding 50 K, with even a third m/z 91 fragment appearing with a ratio of 0.3. This confirms the hypothesis of a lower energy barrier to fragmentation than for Trp. These values demonstrate that for α-amino acids, the vaporization temperature is the most critical parameter to be adjusted in order to avoid thermal energy transfer to the neutral molecule, and obtain fragment-free mass spectra, when the photon energy is set below the dissociative ionization onset of "cold molecules".

As for Trp, Fig. 11 shows the experimental TPES (blue curve), derived from the TPEPICO spectrum presented in Fig. 9, with a total resolution of 27 meV. The phenylalanine TPES is composed of four parts: the onset region followed by three broad bands with maxima located approximately at 10.1, 10.7 and 11.5 eV. The convoluted stick diagram is calculated as described above for T = 423 K and corresponds to the ionization of molecular orbitals of the three most stable Phe conformers (CF1, CF2(1) and CF2(2)).[44] In this energy range 5 MOs can be ionized according to the IE calculations of Dehareng and Dive.[44] As it is the case for Trp, π-like molecular orbitals involved in the ionization of the different conformers have ionization energies in the onset region. But from the TPEPICO spectra, these MOs are not involved in the rupture of the Cα–Cβ bond but rather lead to a fragment corresponding to the loss of the COOH group appearing near the threshold (m/z = 120). The first band, with a maximum in the 9.5–10.5 eV region, is likely to correspond to lone-pair and σ orbitals localized on the backbone and between Cα and Cβ. In this region, the fragments (m/z = 91 and 74) corresponding to the break of the Cα–Cβ bond are both present, with the charge localisation in the heaviest fragment (m/z = 91) being more stable by ~300 meV. The second broad TPES band, starting at 10.5 eV, involves an antibonding combination of a π density on C=O and a lone-pair part localized on the oxygen of the O–H group, as well as a sigma Cα–Cβ orbital. The ionization of the molecular orbital described by a π-type MO with a highdensity on C=O and σ bonds localized on several C–C and C–H of the side chain of the first CF1 conformer contributes to the end of the spectrum (~11.4 eV) according to Dehareng and Dive.[44] In this last region, the predominant fragment is the lightest product of the Cα–Cβ bond break. As mentioned for Trp, the multitude of Phe conformations involved does probably not permit to obtain a more structured spectrum. However, the observed TPES band structure can be nicely correlated to specific ionized molecular orbital groups in the case of Phe in good consistency with the calculations from ref. 44. As in the case of Trp,

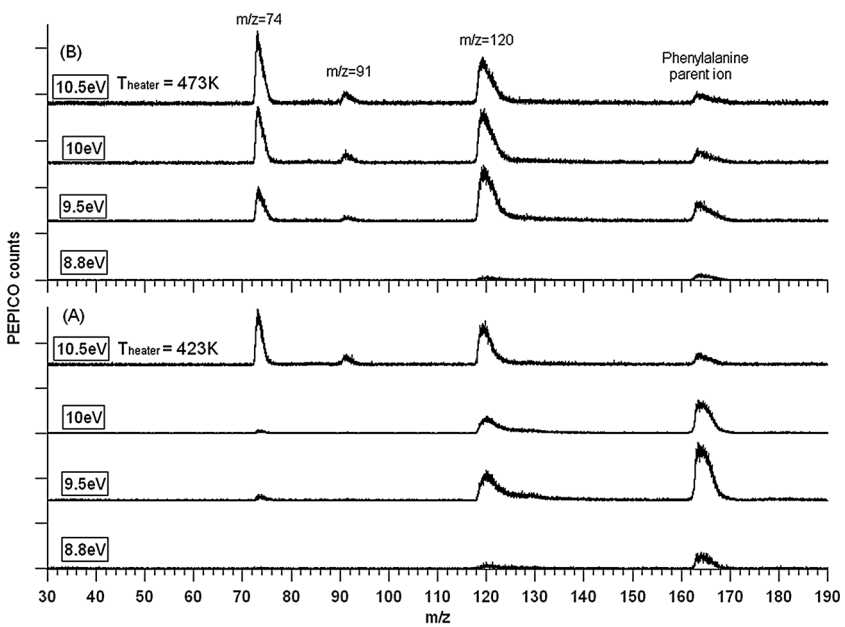

Fig. 10 PEPICO mass spectra of phenylalanine obtained at 8.8, 9.5, 10 and 10.5 eV at two temperatures: (A) 423 K, (B) 473 K.

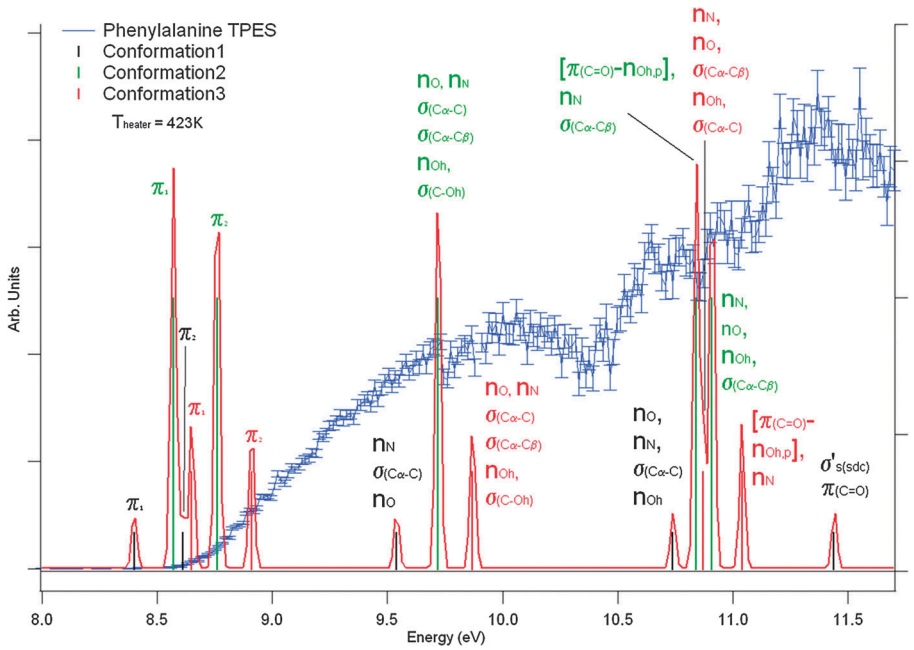

Fig. 11 TPES of phenylalanine with a total resolution of 27 meV (blue curve); the black, green and red stick diagrams are related to OVGF calculations of the three most stable phenylalanine conformers (see text): Conformation 1 = CF1, Conformation 2 = CF2(1), Conformation 3 = CF2(2);[47] the red curve corresponds to the convolution between the stick diagram and our total spectral resolution (27 meV here).

the lack of structure and the precision of the theoretical methods render the extraction of conformer populations impossible. However, this tentative conclusion must be verified by a complete TPES simulation using conformer dependent FCF calculations.

Finally, we can also compare our work to the two-color R2PI measurements of conformer dependent ionization energies performed by Lee *et al.*,[38] who fixed the first laser to six known conformer specific S_1 band origins, respectively, and then scanned the 2nd ionizing laser photon for each S_1 energy. They find ionization energies in the range of 8.80 to 9.15 eV for the six different conformers of their jet-cooled L-Phe sample. No error is given in their work but from their Fig. 3, the error can be estimated to be about 50 meV. Interestingly, none of their six conformers can be ionized at our experimental value of 8.63 ± 0.02 eV, our experimental IE being considerably lower than those of Lee *et al.*, by 170 meV at minimum. If one admits that the IE does not (or marginally) depend on temperature for such large molecules (*cf.* discussion in ref. 42), this would mean that, in our 423 K sample, different conformers with lower IEs are abundant too as compared to the jet-cooled molecules, which is reasonable to assume. However, considering that their 8.80 eV IE value is in disagreement with the values from ref. 25 and 45, and from the present work, all obtained *via* single photon ionization, one could wonder if the higher value reported by Lee *et al.* is due to the R2PI process involving different FCFs because of the presence of the intermediate S_1 neutral state.

3. Conclusion and perspectives

We presented an aerosol source with a nanoparticle flash-vaporization module implemented for the first time inside a VMI/WM-TOF photoelectron/photoion coincidence (PEPICO) spectrometer operating with VUV synchrotron radiation. This detection scheme provides several advantages over conventional mass spectrometers, such as the analysis of the electronic structure with high resolution, versatility, and the preparation of state selected ions when operated in threshold coincidence mode. In addition, we manage to achieve a high density of thermodesorbed molecules allowing to work with the first order light of the grating's monochromator. Aerosol thermal desorption is a soft vaporization method and has been used here to study the VUV spectroscopy of thermally-fragile α-amino acids, tryptophan and phenylalanine. We were able to obtain fragment-free mass spectra of these biomolecules and to record the first Threshold Photoelectron/Photoion Coincidence (TPEPICO) spectra of these compounds. Thermochemical values such as ionization and appearance energies were obtained for the two amino acids, lowering the incertitude on the values by a factor of 4 and 5, respectively, as compared to previous works. In the case of Phe, fragments AE values of m/z 120, 91 and 74 have been reported here for the first time.

TPES spectra of the two molecules, with 53 and 27 meV total resolution respectively, have been compared to theoretical calculations on vertical ionization energies performed by Dehareng and Dive.[44] The spectra show fairly broad bands which is rationalized by the superposition of TPES spectra of a broad population of conformers in our sample. But this hypothesis has to be verified by experimental spectra at even higher resolution. For both molecules, the observed TPES bands coincide nicely with ionization energies of MOs given in ref. 44. However, in order to quantitatively simulate TPES spectra, one needs quantum chemical calculations of conformer-dependent Franck–Condon factors. Nevertheless, comparison with the TPEPICO spectra allowed correlating the nature of the involved MOs with the fragmentation pattern.

Compared to other experiments using heated ovens to vaporize biomolecules, the quantity of commercially available or synthesized compounds used during an aerosol experiment is considerably reduced. More precisely, only a few tens of milligrams are used for a 24 hour experiment, a critical advantage if one wants to study molecules difficult to synthesize or commercially expensive.

In addition, we have demonstrated the ability to control the thermal energy imparted to the neutral molecule during the vaporization process by optimizing the TD temperature.

The present setup is currently being applied to the study of photon-induced processes on natural and modified nucleobases (NAB)[47] showing the versatility of the method and its relevance for future experiments on other biomolecules, such as oligopeptides and for analytical chemistry using atmospheric-pressure photoionization (APPI) for example.

With the use of the thermal desorption module, future experiments on atmospheric aerosols chemical composition, such as secondary organic aerosol (SOA) produced in a smog chamber on the DESIRS beamline, are foreseen. The insertion of a differential mobility analyzer (DMA) is also envisaged in the short term, in order to size-select the SOAs prior to the thermodesorption and obtain richer information on their production and composition. The DMA will also be used for the study of circular dichroism of nanometre-sized aerosol particles and, more generally, for the study of the angular distribution of photoelectrons emitted from nanoparticles, such as those obtained for DOP nanoparticles.

Acknowledgements

We gratefully acknowledge financial support by the French Groupe de Recherche "exobiologie" (which has become the "Société Francaise d'Exobiologie" today) as well as the CNRS Interdisciplinary programme "Evironnements planétaires et Origine de la Vie". We thank Sydney Leach and Didier Despois for helpful discussions. We are strongly indebted to Jean-François Gil for his help in the design and the mounting of the thermodesorber. We would also like to thank the general technical staff of SOLEIL for running the facility.

References

1 J. P. Schermann, *Spectroscopy and Modeling of Biomolecular Building Blocks*, Elsevier Science Ltd, 2008.
2 J. Šponer and F. Lankaš, *Computational Studies of RNA and DNA*, Springer Series Challenges and Advances in Computational Chemistry and Physics, 2006, vol. 2.
3 D. Despois, Biological Molecules, in *"Hunt for molecules"*, ed. F. Combes, F. Casoli and L. Pagani, Paris Observatory Publications, 2005; *Lectures in Astrobiology*, ed. M. Gargaud, B. Barbier, H. Martin and J. Reisse, Springer Series "Advances in Astrobiology and Biogeophysics", Springer, Berlin Heidelberg, 2005; E. Herbst, *Chem. Soc. Rev.*, 2001, **30**, 168–176.
4 P. Ehrenfreund, M. P. Bernstein, J. P. Dworkin, S. A. Sandford and L. J. Allamandola, *Astrophys. J.*, 2001, **550**, L95–L99; Z. Peeters, O. Botta, R. Ruiterkamp and P. Ehrenfreund, *Astrophys. J.*, 2003, **593**, L129–L132.
5 M. Schwell, H. W. Jochims, H. Baumgärtel, F. Dulieu and S. Leach, *Planet. Space Sci.*, 2006, **54**, 1073.
6 S. Pilling, D. P. P. Andrade, R. B. deCastilho, R. L. Cavasso-Filho, A. F. Lago, L. H. Coutinho, G. G. B. deSouza, H. M. Boechat-Roberty and A. Naves de Brito, *Proceedings of the International Astronomical Union*, 2008, **V4**(Symposium S251), 371.
7 T. P. Debies and J. W. Rabalais, *J. Electron Spectrosc. Relat. Phenom.*, 1974, **3**, 315.
8 P. H. Cannington and N. S. Ham, *J. Electron Spectrosc. Relat. Phenom.*, 1983, **32**, 139.
9 M. Whitehouse, R. N. Dreyer, M. Yamashita and J. B. Fenn, *Anal. Chem.*, 1985, **57**, 675; M. Yamashita and J. B. Fenn, *J. Phys. Chem.*, 1984, **88**, 4451.
10 F. Hillenkamp and K. P. Katalinic, *A practical guide to MALDI MS Instrumentation, methods & applications*, Wiley-VCH, 2006.
11 D. Nolting, C. Marian and R. Weinkauf, *Phys. Chem. Chem. Phys.*, 2004, **6**, 2633.
12 H. Kang, C. Dedonder-Lardeux, C. Jouvet, S. Martrenchard, G. Grégoire, D. Desfrançois, J.-P. Schermann, M. Barat and J. A. Fayeton, *Phys. Chem. Chem. Phys.*, 2004, **6**, 2628; H. Kang, C. Jouvet, C. Dedonder-Lardeux, S. Martrenchard, G. Grégoire, D. Desfrançois, J.-P. Schermann, M. Barat and J. A. Fayeton, *Phys. Chem. Chem. Phys.*, 2005, **7**, 394.
13 F. Piuzzi, I. Dimicoli, M. Mons, B. Tardivel and Q. Zhao, *Chem. Phys. Lett.*, 2000, **320**, 282.
14 J. Zhou, O. Kostko, C. Nicolas, X. Tang, L. Belau, M. S. de Vries and M. Ahmed, *J. Phys. Chem. A*, 2009, **113**, 4829.
15 R. C. Sullivan and K. A. Prather, *Anal. Chem.*, 2005, **77**, 3861.
16 M. Bente, T. Adam, T. Ferge, S. Gallavardin, M. Sklorz, T. Streibel and R. Zimmermann, *Int. J. Mass Spectrom.*, 2006, **258**, 86.
17 F. Gaie-Levrel, S. Perrier, E. Perraudin, C. Stoll, N. Grand and M. Schwell, to be submitted.
18 J. Cabalo, A. Zelenyuk, T. Baer and R. E. Miller, *Aerosol Sci. Technol.*, 2000, **33**, 3.
19 D. C. Sykes, E. Woods, G. D. Smith, T. Baer and R. E. Miller, *Anal. Chem.*, 2002, **74**, 2048.
20 E. Woods, G. D. Smith, Y. Dessiaterik, T. Baer and R. E. Miller, *Anal. Chem.*, 2001, **73**, 2317.
21 M. J. Northway, J. T. Jayne, D. W. Toohey, M. R. Canagaratna, A. Trimborn, K. I. Akiyama, A. Shimono, J. L. Jimenez, P. F. DeCarlo, K. R. Wilson and D. R. Worsnop, *Aerosol Sci. Technol.*, 2007, **41**, 828.
22 J. Shu, S. Gao and Y. Li, *Aerosol Sci. Technol.*, 2008, **42**, 110.
23 E. R. Mysak, K. R. Wilson, M. Jimenez-Cruz, M. Ahmed and T. Baer, *Anal. Chem.*, 2005, **77**, 5953.
24 J. Shu, K. R. Wilson, M. Ahmed and S. R. Leone, *Rev. Sci. Instrum.*, 2006, **77**, 043106.
25 K. R. Wilson, M. Jimenez-Cruz, C. Nicolas, L. Belau, S. R. Leone and M. Ahmed, *J. Phys. Chem. A*, 2006, **110**, 2106.
26 K. R. Wilson, D. S. Peterka, M. Jimenez-Cruz, S. R. Leone and M. Ahmed, *Phys. Chem. Chem. Phys.*, 2006, **8**, 1884.
27 G. A. Garcia, H. Soldi-Lose and L. Nahon, *Rev. Sci. Instrum.*, 2009, **80**, 023102.
28 A. T. J. B. Eppink and D. H. Parker, *Rev. Sci. Instrum.*, 1997, **68**, 3477.
29 See http://www.synchrotron-soleil.fr/Recherche/LignesLumiere/DESIRS.
30 I. Powis, *Advances in Chemical Physics*, ed. J. C. Light, 2007, Wiley, New York.
31 L. Nahon, G. Garcia, I. Powis, U. Meierhenrichch and A. Brack, *SPIE Proceedings: Instruments Methods and Missions for Astrobiology X*, 2007, **6694**, 69403.
32 M. Richard-Viard, A. Delboulbe and M. Vervloet, *Chem. Phys.*, 1996, **209**(2–3), 159.
33 X. Wang and P. H. McMurry, *Aerosol Sci. Technol.*, 2006, **40**, 320.
34 O. Marcouille, P. Brunelle, O. Chubar, F. Marteau, M. Massal, L. Nahon, K. Tavakoli, J. Veteran and J.-M. Filhol, *Synchrotron Radiation Instrumentation*, Pts 1 and 2, ed. J. Y. Choi and S. Rah, AIP, New York, 2007, vol. 879, p. 311.
35 L. Nahon, C. Alcaraz, J.-L. Marlats, B. Lagarde, F. Polack, R. Thissen, D. Lepère and K. Ito, *Rev. Sci. Instrum.*, 2001, **72**, 1320.
36 B. Mercier, M. Compin, C. Prevost, G. Bellec, R. Thissen, O. Dutuit and L. Nahon, *J. Vac. Sci. Technol., A.*, 2000, **18**, 2533.
37 T. R. Rizzo, Y. D. Park, L. A. Peteanu and D. H. Levy, *J. Chem. Phys.*, 1985, **84**, 2534.
38 K. T. Lee, J. Sung, K. J. Lee, Y. D. Park and S. K. Kim, *Angew. Chem., Int. Ed.*, 2002, **41**, 4114.
39 K. R. Wilson, S. Zou, J. Shu, E. Rühl, S. R. Leone, G. C. Schatz and M. Ahmed, *Nano Lett.*, 2007, **7**, 2014.

40 K. Seki and H. Inokuchi, *Chem. Phys. Lett.*, 1979, **65**, 158.
41 S. Campbell, J. L. Beauchamp, M. Rempe and D. L. Lichtenberger, *Int. J. Mass Spectrom. Ion Processes*, 1992, **117**, 83.
42 W. Genuit and N. M. M. Nibbering, *Int. J. Mass Spectrom. Ion Processes*, 1986, **73**, 61.
43 B. Sztaray, A. Bodi and T. Baer, Modeling unimolecular reactions in photoelectron photoion coincidence experiments, *J. Mass Spectrom.*, 2010, **45**, 1233.
44 D. Dehareng and G. Dive, *Int. J. Mol. Sci.*, 2004, **5**, 301.
45 S. Campbell, E. M. Marzluff, M. T. Rodgers, J. L. Beauchamp, M. E. Rempe, K. F. Schwinck and D. L. Lichtenbergert, *J. Am. Chem. Soc.*, 1994, **116**, 5257.
46 L. C. Snoek, E. G. Robertson, R. T. Kroemer and J. P. Simons, *Chem. Phys. Lett.*, 2000, **321**, 49.
47 F. Gaie-Levrel, D. Touboul, G. Garcia, L. Nahon and M. Schwell, manuscript in preparation.

